Effect of montmorillonite on morphology, glass transition and crystallinity of the Xylitol-plasticized bionanocomposites

Huihua Liu[1], Deeptangshu Chaudhary[2] ●

1 School of Health Sciences, University of Ballarat, Mount Helen, VIC 3350, Australia

2 Department of Chemical Engineering, Curtin University of Technology, Perth, Australia

h.liu@ballarat.edu.au and d.chaudhary@curtin.edu.au,

• Corresponding author, phone: +61 +61 8 92662522; Fax: +61 8 92662681

Abstract

High amylose based nanocomposites plasticized by xylitol were prepared via twin-screw extrusion. The synergistic interaction in the xylitol-plasticized nanocomposite was studied via various characterization methods and the unique behavior of the xylitol-plasticized nanocomposite had been discussed. As revealed in the XRD and TEM results, good intercalated/exfoliated morphology had been achieved in all the nanocomposites. Furthermore, the expansion of nanoclay basal spacing was related to the xylitol/nanoclay ratio. DSC analysis clearly proved the unique crystallization process of xylitol-plasticized samples. Moreover, in the crystallization domain results, two domains sized at approximately 93.7Å and 346Å were found. This observation points to a two-level complex effect from two aggregate domains; one, the re-aggregation of certain number of silicate layers into domains which trap some of the amylose polymer chains, and two, the bulk drying process which combines smaller amylose crystalline domains within a larger amorphous high amylose matrix.

Keywords: nanocomposite; starch; xylitol; XRD; SAXS; DSC

1 Introduction

Continuous interests have been drawn on the research related to the starch-based bionanocomposites in response to the blooming demands of material with tailored-properties (Kampeerapappun, Aht-ong, Pentrakoon & Srikulkit, 2007; Qiao, Tang & Sun, 2010; Rhim, 2011). Investigations on using nanoclay as the reinforcing phase, on account of their very high aspect ratio (100) and versatility (Rhim, Lee & Hong, 2011; Wang, Zhang, Han & Bai, 2009; Xiong, Tang, Tang & Zou, 2008) have been widely carried out in the last decades. Most studies are focused on the examinations of the properties, mechanisms, and aiming for fabrication of properties-tailored materials via introducing different plasticizers (Averous, 2007; Follain, Joly, Dole, Roge & Mathlouthi, 2006; Rhim, 2011) with the aim to manipulate the bulk properties of the prepared composites. The dominant factor pertain to its relevant properties is the synergistic interactions in terms of basal spacing, crystallinity value, moisture content and hydrogen bonding changes among plasticizer/starch/nanoclay within the hydrophilic system. In a polysaccharide-based polymeric system, hydrogen bond is the most important bond and the interactions associated with it are complex and hardly well documented due to the intricate nature of such macromolecules. Therefore, most studies target to alter or balance the –OH related interaction from a molecular level, such as incorporating different type (based on different affinity) of smaller molecule hydrophilic plasticizer. As we have described before(Chaudhary & Liu, 2012; Liu et al., 2012), All the mentioned factors are believed to be of utmost importance in affecting and determining the synergistic interactions in such hydrophilic polymeric network which are in turn reflected as the different reported values in crystallinity, mechanical properties, and glass-transition temperature for nanocomposite plasticized by different plasticizers in literatures (Tang & Alavi, 2011). Although many studies had been published in the last few decades, a direct comparison of the various results in often difficult because most starch biopolymer based systems are complex in nature due to their varying ratio of amylopectin and amylose, presence of plasticizer and the processing conditions and

water activity of the final product tend to affect the characterization results. In such context, under same processing condition, we studied two different plasticizers based on number of -OH group (glycerol and sorbitol) to illustrate the effect of the hydrophilicity, stereo-conformation, water activity on the final retrogradation behavior of the starch biopolymer matrix (Liu, Chaudhary, Yusa & Tadé, 2011b). Those studies highlighted the importance of the number of hydroxyl groups , molecule size and the intrinsic properties of the plasticizer in manipulating the synergistic interactions thereof (Chaudhary, 2010; Chaudhary, Adhikari & Kasapis, 2010; Liu, Chaudhary, Yusa & Tadé, 2011a, b) which were reflected as bulk properties such as crystallinity, glass-transition temperature and extent of 'locked' moisture as seen through bonding changes in FTIR spectra etc.

In this study, to further understand the impact of type of plasticizer on the properties of nanocomposites, a five –OH group plasticizer, xylitol, is investigated. Comprehensive characterization works were carried out including XRD, DSC and synchrotron measurements. Particular attentions were paid to distinguishing the behavior of xylitol-plasticized bionanocomposites in this study, when compared to the glycerol and/or sorbitol plasticized nanocomposites (based on our previous publications).

2 Material and Method

2.1 Materials, nomenclature and processing

High-Amylose starch (about 70% amylose), HA-starch, was purchased from National Starch Company (New Jersey, USA), xylitol was obtained from Food Dept Ltd. (Melbourne, Australia) and nanoclay (99.5% pure) was generously supplied by NichePlas Ltd. (Sydney, Australia). 11 samples were prepared at different ratio of nanoclay/xylitol concentration. Each formulation was presented as a label such as X105, where 'X' refers to the plasticizer type (xylitol, in the current work), the first digit, '1', refers to the nanoclay content in weight percent (e.g., 1 wt% in X105) and the last two digits '05' refer to the weight percent of xylitol within the sample. The

sample nomenclatures are listed in Table 1, where PS refers to the HA-starch sample.

2.2 Characterization

2.2.1 X-ray diffraction

XRD measurements of the prepared samples were performed in a Bruker Discover 8 diffractometer operating at 40kV and 40mA with a 2θ range from 3° to 30° at a scanning rate of 0.5 °/sec. The basal spacing of the nanoclay was determined from the Bragg's equation, $\lambda=2d\sin\theta$ (where θ is the diffraction position and λ is the wavelength). The d-spacing for the pristine nanoclay used in the current study is 11.7Å as provided by the supplier.

2.2.2 Transmission electron microscopy

TEM was performed on ultrathin sections, 150nm in thickness, at JEM-2100 microscope (JEOL, Tokyo, Japan), operating at an accelerating voltage of 200 kV. The representative samples were sectioned at room temperature with diamond knife using a Leica Ultramicrotome (EM UC7, Tokyo, Japan). The obtained sections were sandwiched between two 400-mesh copper grids for TEM observation.

2.2.3 Measurement of glass transition temprature (Tg)

DSC measurement was performed on SEIKO 6200 (Seiko, Japan). About 10mg sample was placed in an aluminum sealed sample pan. The sample was heated from -50°C to 250°C at a heating rate of 5°C /min, kept at 250°C for 1 minutes followed by cooling down to 25°C at 10°C /min. The glass transition temperature (T_g) was taken as the inflection point of the increment of specific heat capacity. Melting temperature was recorded for analysis as well.

2.2.4 Synchrotron measurements

Synchrotron beamline BL40B2(Inoue, Oka, Miura & Yagi, 2004) at SPring-8 synchrotron facility (Hyogo, Japan) was used to characterize the prepared samples via Small Angle X-ray Scattering technique (SAXS). One aluminum filter block was

employed to decrease the strength of the X-ray so as to obtain an optimized pattern. The beam was monochromatized to a wavelength of 0.1 nm with an object distance of 1151.76mm. All patterns were recorded on a CCD camera that was calibrated by the diffraction rings from an AgBH (silver behenate) reference sample. The measurement time per sample was chosen to eliminate the radiation damage on the tested samples, which was subsequently determined to be 10 seconds. The diffraction profiles were normalized to the beam intensity and corrected using an empty background. The data reduction of the 2-D X-ray scattering patterns was completed with NIKA macros (Ilavsky & Jemian, 2009) based on Igor 6.02 (Wavemetrics, Lake Oswego, Oregon).

Using the low Q region from the SAXS data, valuable information on the size distribution of crystalline fractions within the polymer could be determined. The Maximum Entropy Method (MEM) developed by Potton *et al.*(Potton, Daniell & Rainford, 1988) for Irena modeling macros (Ilavsky & Jemian, 2009) was employed to understand and quantify the crystalline domain morphologies within the polymer system (Potton, Daniell & Rainford, 1988).

3 Result and Discussion

3.1 XRD results

The XRD patterns for the prepared samples, in Figure 1(a), showed that the *basal spacing (d-spacing)* of all the samples increased to different extents regardless of the nanoclay content. The *basal spacing* value also suggested that starch and/or xylitol molecules had successfully migrated into the gallery of nanoclay. Meanwhile, the TEM images for the representative samples (X210 and X420) are shown in Figure 1 which indicated that most of the samples achieved mixed morphologies (intercalated/exfoliated co-existed).

It could be also read from Table 1 that, when the nanoclay concentration is fixed, the *d-spacing* value increased upon increasing the xylitol content, except the 4% nanoclay sample where d_{X420}(17.6 Å) is slightly smaller than d_{X410}(17.9 Å). There is no obvious

trend that could be found when comparing the sample with different concentration of nanoclay for same xylitol concentration, and this is different to what was reported in the glycerol/sorbitol plasticized samples where a positive trend between increase in nanoclay concentration and increases in the *d-spacing* can be seen (Liu, Chaudhary, Yusa & Tadé, 2011a, b).

The MMT characteristic peak occurred in all the samples with xylitol concentration less than 10% (X105, X210, X305 and X410). This observation was different to what was found in the glycerol- and sorbitol-plasticized samples (Liu, Chaudhary, Yusa & Tadé, 2011a, b), where such peak broadening occurred in the 5% plasticizer loading samples only. In other words, more xylitol (10% compared to 5% in glycerol/sorbitol samples) is required to achieve the same amount of well-formed crystal structure (sharp peak) arrangement as observed from the XRD measurement. When compared to glycerol behavior, this suggested that xylitol hinders the formation of crystal structure with xylitol/MMT/amylose at low plasticizer concentration. In other words, when the xylitol amount is less than 10%, the nucleation is relatively more heterogeneous as reflected as the broaden peak in the corresponding samples. However, when the concentration is greater than 10%wt, the XRD data can be interpreted which indicates that relatively greater uniformity in the crystal structure existed in xylitol-plasticized systems compared to that from glycerol/sorbitol sample at same plasticizer level. We think that one reason behind this is the strong plasticizer/plasticizer interaction of xylitol which enhanced the extent of nanoclay intercalation with the amylose polymer and thus sustained uniform crystal growth. This is further discussed in the crystallization section.

Furthermore, as shown in Table 1, the *basal spacing* for different samples is overall larger than that from glycerol-plasticized nanocomposites but smaller than sorbitol-plasticized sample. Such results clearly indicated that the expansion degree of the nanoclay gallery is related to the size of the plasticizer incorporated in the complex system. In other words, the *d-spacing* was primarily determined from the

molecular size of the plasticizer. This is consistent with the findings in our previous publications on the glycerol/sorbitol plasticizer nanocomposites.

3.2 Crystallinity analysis

The crystallinity results of the prepared samples showed some very interesting results, especially for the application of flexible and clear packaging materials. The composites crystallinity was determined from the XRD patterns based on the method introduced in the previous publication (Lopez‐Rubio, Flanagan, Gilbert & Gidley, 2008), the results are shown in Table 1, standard deviations for crystallinity calculations are within ± 1%. There are two main factors affecting the crystallinity (X_c%) of the composites, they are nanoclay and plasticizer concentrations and it is well known that increasing nanoclay concentration enhances polymer crystallinity due to its typical nucleation effect, whereas increasing the amount of plasticizer decreased overall crystalline structure through typical plasticization.

The native crystallinity obtained for high amylose starch is around 10%, and we have reported in our earlier work that our samples of high amylose starch from corn showed around 8% bulk crystallinity (Liu, Chaudhary, Yusa & Tadé, 2011b). It has also been reported that crystallinity values are extremely important to understand starch retrogradation, where the bulk crystallinity can increase up to 20%. As shown in Table 1, the incorporation of nanoclay tends to increase the crystallinity slightly, primarily due to the nucleating effect. However, it is also well known that not only nanoclay, which is very important for enhanced physical/barrier properties, plasticizers are needed to improve the flexibility and optical clarity of the amylose polymer (in the form of thin films), but higher nanoclay concentration possess a dispersion issue and higher plasticizer concentration increases the retrogradation behavior. Therefore, it is very interesting to observe that as we increased the nanoclay and xylitol concentration, their interplay and their interactions with the amylose polymer balanced the bulk crystallinity. It was also found that the crystallinity value

of xylitol-plasticized sample were significantly higher than that from glycerol/sorbitol-plasticized ones.

This finding is very important for the application of such biopolymer nanocomposites in the field of packaging because the two observations regarding nanoclay characteristic peak occurred at higher xylitol concentration (higher than 10%) and overall higher and stable crystallinity values of the nanocomposites suggested that the xylitol-plasticized system increases the threshold crystallinity of the bulk matrix, and prevents further polymer reorganization and thus starch retrogradation.

3.3 Avrami Equation analyses based on DSC-crystallization mechanism

As widely known, in polymer–clay systems, the endotherm peak can provide information on the crystalline phases in the nanocomposites when the clay platelets have nano-scale interactions. To gain an improved understanding of these interactions on the bionanocomposites' crystallization behavior, the crystallization process was modeled as a combination of several infinitesimal isothermal steps (Lee et al., 1999). The Avrami equation (Eq 1), which is widely applied in investigating crystallization behaviors of polymer systems (Lee et al., 1999), was employed to study the non-isothermal crystallization kinetics of the prepared bionanocomposites

$$X_t = \int_{t_0}^{t} \frac{dH_c}{dt} dt \Big/ \int_{t_0}^{t_\infty} \frac{dH_c}{dt} dt \quad (1)$$

All the curves had a partial sigmoid shape, and the analysis of the development of relative crystallinity could be obtained using $X_t = 1 - \exp(-kt^n)$. A plot of $log[-ln(1 - Xt)]$ vs. $log(t)$ could provide n, the value depending upon the mechanics of nucleation and the form of crystal growth, and k, a rate constant containing the nucleation and growth parameters. The exponent n and the factor k from Avrami Equation analyses are presented in Table 2.

The n values for the composite samples increased with increasing the xylitol c% at each fixed MMT amount; same finding was observed with increasing MMT amount

at fixed xylitol concentration. Because a lower *n* (composites) compared to *n* (PS) indicated the more heterogeneous nucleation. It could be read that, the *n* value for <10% xylitol samples are overall smaller (more heterogeneous nucleation) than that for the >10% xylitol samples. This mutually support the finding from XRD that <10% xylitol samples showed broaden peak in XRD pattern (corroborate with the finding more heterogeneous nucleation). Furthermore, clearly, the increasing of MMT amount led to an increased in *n* value which means the nucleation process is becoming relatively homogenous (higher n value in high MMT samples). this observation could be explained based on the well-known nucleation effect of MMT which is becoming the dominant role in a MMT-rich scenario which balanced the competitive nucleation effect from xylitol and led to relatively homogenous nucleation process. On the other hand, the next factor *k* (related to the rate of crystal growth), which showed a large variation. The high xylitol samples showed an overall lower value than that from the low xylitol samples regardless the amount of MMT presented.

3.4 Synchrotron results

Specific models have been developed for SAXS data analysis in different characteristic systems (Roe, 2000). The background of the sample holder was subtracted from the raw 2-D X-ray diffraction patterns for representative composites, as shown in Figure 2.

As shown in Figure 2 the scattering patterns (shape and the intensity) of different samples were greatly influenced by varying the loading of nanoclay and/or xylitol. The shape of the scattering pattern changed from approximately circular (X105) to obviously elliptical (X410), which reflected the growth of lamellar structure/ crystalline domains within the composites. The SAXS profiles for the obtained samples are shown in Figure 3.

From Figure 3, the sharp d_{001} in high xylitol content (15% and 20% xylitol) samples strongly indicated a closely packed structure of polymer-MMT and polymer-xylitol

assemblages. In other words, 10% xylitol acted like the critical point in determining the morphologies of corresponding nanocomposites which is mutually agree with the suggestion from XRD analysis where only broad peaks were observed in samples containing less than 10% xylitol. Samples with xylitol content larger than 10% tended to show an overall tighter molecular packing within the polymeric network regardless the nanoclay loading. Furthermore, it has been suggested that a closely packed starch network was an indication of lower polymer chain mobility (Vodovotz & Chinachoti, 1998). This could be linked back to the high T_m values observed for the high xylitol samples where high xylitol samples showed higher T_m value compared with that from low xylitol samples.

3.5 Size distribution of the crystalline domains

Two domains were observed in all samples, where the diameters of scatters were denoted as $\bar{d}_1$ (around 104.1Å) and $\bar{d}_2$ (around 350.5Å), Table 3. This finding initiated the assumption that, the interaction in this complex polymeric system could be considered as a two scale interaction which led to two different crystalline domains at two different size ($\bar{d}_1$ and $\bar{d}_2$). Firstly, the smaller molecular components (xylitol/MMT) start to form crystals at a smaller size $\bar{d}_1$ (around 100 Å), after that, the dominate rearrangement of starch chains at a larger-scale promoted the formation of the second larger size crystalline domain $\bar{d}_2$.

As shown in Table 3, the mean scatter diameter for $\bar{d}_1$ ranged from 95.3Å to 119.4Å and the crystal size increased as increasing the MMT concentration except in 1% MMT samples. This indicated that the crystallize domain size is primarily depended on the MMT amount, where larger MMT amount led to slightly bigger crystalline size during the first stage of crystallization process ($\bar{d}_1$) where the smaller molecular components (xylitol/MMT) start to form crystals at a smaller size. We can relate this to the finding from XRD and TEM that the higher degree of intercalation are found

when increasing the MMT concentration. Higher degree of intercalation is resulted from the enhanced the MMT/xylitol interaction. On the other hand, the enhanced MMT/xylitol interaction could in turn slightly increase the size of the crystal assemblage as well as shown in Table 3. Furthermore, when increasing the xylitol amount at a fixed MMT%, the MMT/xylitol interactions might led to the formation of smaller crystalline domains due to the nucleating effect of MMT. Additionally, this was reflected in the reduced scatter diameter with changing xylitol concentrations.

It had been reported that the formation of another larger size domains could be correlated to the well-defined retrogradation phenomenon, where the rearrangement of amylose chains at a larger-scale becomes a dominant process during ageing (Farhat, Blanshard & Mitchell, 2000). As showed in Table 3, $\bar{d}_2$ value (possibly the rearrangement of the starch polymer chains) is affected by the amount of MMT and xylitol, where increasing MMT% decreased the $\bar{d}_2$ value to different extent. Meanwhile, increasing xylitol amount at a fixed MMT% decreased the $\bar{d}_2$ value as well. Further, the presence of MMT provides local sites for polymer aggregation and leads to the formation of larger domains. In other words, emergence of the larger crystalline domain is the combined effect of, first the re-aggregation of certain number of silicate layers in to ordered domains during drying (Jasmund & Lagaly, 1993) and second, the retrogradation of the high-amylose starch polymer which caused the reorganization of the polymer chains. This is well comply with the hypothesis put forwarded earlier that the interactions in this complex system should be treated as a two-level process. Such observations suggested that the crystallization domain formation in the complex ternary system is system-specific progress that as a result of the interplay of the two-way interactions such as starch/plasticizer, starch/MMT, MMT/plasticizer and the interactions within the same component.

4 Conclusion

The synergistic interaction in the xylitol-plasticized nanocomposite was studied via various characterization methods and the unique behavior of the xylitol-plasticized nanocomposite had been discussed. Based on the results from XRD, it could be concluded that the achievable basal spacing of nanoclay was primarily determined from the molecular size of the plasticizer. Compared to the glycerol and sorbitol plasticized samples, the two observations (high X_c% and broadening of XRD patterns at higher xylitol loading) strongly suggested that in xylitol-plasticized system, the form of crystal were likely to be slower (broadened XRD pattern) due to the competitive nucleation effect from both xylitol and MMT, but the total amount of crystal, higher X_c % values.

Compared to glycerol/sorbitol plasticized samples, as revealed from the DSC results, starch/xylitol/nanoclay nanocomposite tended to from a firmer polymeric network in terms of molecular mobility within the system. Amylose starch chains in xylitol plasticized samples required larger amount of energy before getting mobilized when compared to the glycerol/sorbitol samples. Two domains sized at approximately 104.1Å and 354.62Å were found. These observations resulted from the combined effect of the re-aggregation of certain number of silicate layers in to ordered domains during drying and the retrogradation behavior of the high-amylose starch polymer.

Acknowledgments

The authors are grateful to Dr. Kyuya Nakagawa, their help in synchrotron experiments. Prof. Martin Saunders and Dr. Jeremy Shaw are gratefully acknowledged for helping with TEM experiments. Acknowledge the internal funding from Curtin University and University of Ballarat led Collaborative Research Network (CRN).

Reference

Averous, L. (2007). Cellulose-based biocomposites: Comparison of different multiphasic systems. *Composite Interfaces, 7*(9), 787-805.

Chaudhary, D. (2010). Competitive plasticization in ternary plasticized starch biopolymer system. *Journal of Applied Polymer Science, 118*(1), 486-495.

Chaudhary, D., Adhikari, B., & Kasapis, S. (2010). Glass transition behaviour of plasticized starch biopolymer system-a modified Gordon-Taylor approach. *Food Hydrocolloids, 25*(1), 114-121.

Chaudhary, D., & Liu, H. (2012). Ultrasonic Treatment and Synthesis of Sugar Alcohol Modified Na^{+}-Montmorillonite Clay. *Ultrasonics Sonochemistry, 20*(1), 63-68.

Farhat, I. A., Blanshard, J. M. V., & Mitchell, J. R. (2000). The retrogradation of waxy maize starch extrudates: Effects of storage temperature and water content. *Biopolymers, 53*(5), 411-422.

Follain, N., Joly, C., Dole, P., Roge, B., & Mathlouthi, M. (2006). Quaternary starch based blends: Influence of a fourth component addition to the starch/water/glycerol system. *Carbohydrate Polymers, 63*(3), 400-407.

Ilavsky, J., & Jemian, P. R. (2009). Irena: tool suite for modeling and analysis of small-angle scattering. *Journal of Applied Crystallography, 42*(2), 347-353.

Inoue, K., Oka, T., Miura, K., & Yagi, N. (2004). Present status of BL40B2 and BL40XU at SPring-8 (Beamlines for small angle X-ray scattering). *Eighth International Conference on Synchrotron Radiation Instrumentation* (Vol. 705, p. 336). San Francisc.

Jasmund, K., & Lagaly, G. (1993). *Tonminerale und Tone: Struktur, Eigenschaften, Anwendungen und Einsatz in Industrie und Umwelt*. Steinkopff.

Kampeerapappun, P., Aht-ong, D., Pentrakoon, D., & Srikulkit, K. (2007). Preparation of cassava starch/montmorillonite composite film. *Carbohydrate Polymers, 67*(2), 155-163.

Lee, S. W., Ree, M., Park, C. E., Jung, Y. K., Park, C. S., Jin, Y. S., & Bae, D. C. (1999). Synthesis and non-isothermal crystallization behaviors of poly(ethylene isophthalate-co-terephthalate)s. *Polymer, 40*(25), 7137-7146.

Liu, H., Chaudhary, D., Roberts, J., Weed, R., Sullivan, J., & Buckman, S. (2012). The interaction in sorbitol-plasticized starch bionanocomposites via positron

annihilation lifetime spectroscopy and small angle X-ray scattering. *Carbohydrate Polymers, 83*(2), 659-664.

Liu, H., Chaudhary, D., Yusa, S., & Tadé, M. O. (2011a). Glycerol/starch/Na+-montmorillonite nanocomposites: A XRD, FTIR, DSC and 1H NMR study. *Carbohydrate Polymers, 83*(4), 1591-1597.

Liu, H., Chaudhary, D., Yusa, S., & Tadé, M. O. (2011b). Preparation and characterization of sorbitol modified nanoclay with high amylose bionanocomposites. *Carbohydrate Polymers, 85*(1), 97-104.

Lopez‐Rubio, A., Flanagan, B. M., Gilbert, E. P., & Gidley, M. J. (2008). A novel approach for calculating starch crystallinity and its correlation with double helix content: A combined XRD and NMR study. *Biopolymers, 89*(9), 761-768.

Potton, J. A., Daniell, G. J., & Rainford, B. D. (1988). A new method for the determination of particle size distributions from small-angle neutron scattering measurements. *Journal of Applied Crystallography, 21*(6), 891-897.

Qiao, X., Tang, Z., & Sun, K. (2010). Plasticization of corn starch by polyol mixtures. *Carbohydrate Polymers, 88*(4), 1172-1176.

Rhim, J. W. (2011). Effect of clay contents on mechanical and water vapor barrier properties of agar-based nanocomposite films. *Carbohydrate Polymers, 86*(2), 691-699.

Rhim, J. W., Lee, S. B., & Hong, S. I. (2011). Preparation and characterization of agar/clay nanocomposite films: the effect of clay type. *Journal of Food Science, 76*(3), N40-N48.

Roe, R. J. (2000). *Methods of X-ray and neutron scattering in polymer science*. Oxford University Press New York.

Tang, X., & Alavi, S. (2011). Recent advances in starch, polyvinyl alcohol based polymer blends, nanocomposites and their biodegradability. *Carbohydrate Polymers, 85*(1), 7-16.

Vodovotz, Y., & Chinachoti, P. (1998). Glassy- Rubbery Transition and Recrystallization during Aging of Wheat Starch Gels. *J. Agric. Food Chem, 46*(2), 446-453.

Wang, N., Zhang, X., Han, N., & Bai, S. (2009). Effect of citric acid and processing on the performance of thermoplastic starch/montmorillonite nanocomposites. *Carbohydrate Polymers, 76*(1), 68-73.

Xiong, H., Tang, S., Tang, H., & Zou, P. (2008). The structure and properties of a starch-based biodegradable film. *Carbohydrate Polymers, 71*(2), 263-268.

Figure Captions

Figure 1 (a) WAXD diffractograms for xylitol – plasticized samples; where the dotted line indicated the position of clay peak in the XRD curve (b) TEM images for X210 and X420

Figure 2 Raw 2-D SAXS patterns for X105/X305 and X210/X410.

Figure 3 SAXS Profiles for xylitol-plasticized samples.

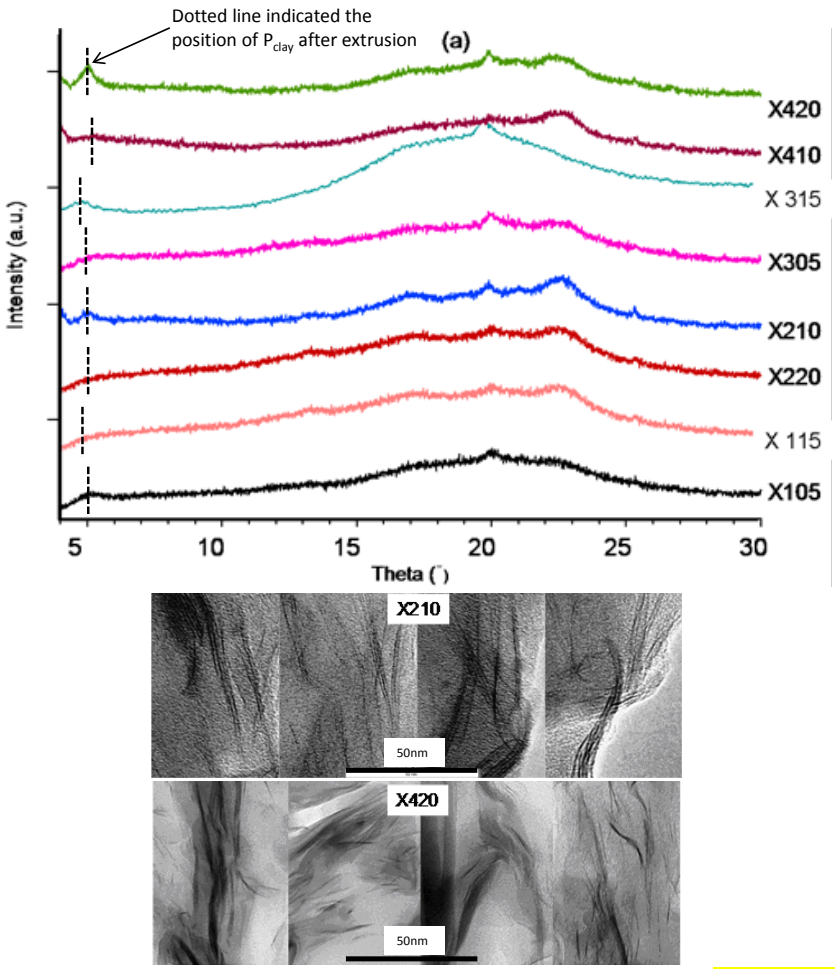

Figure 1 (a) WAXD diffractograms for xylitol – plasticized samples; where the dotted line indicated the position of clay peak in the XRD curve (b) TEM images for X210 and X420.

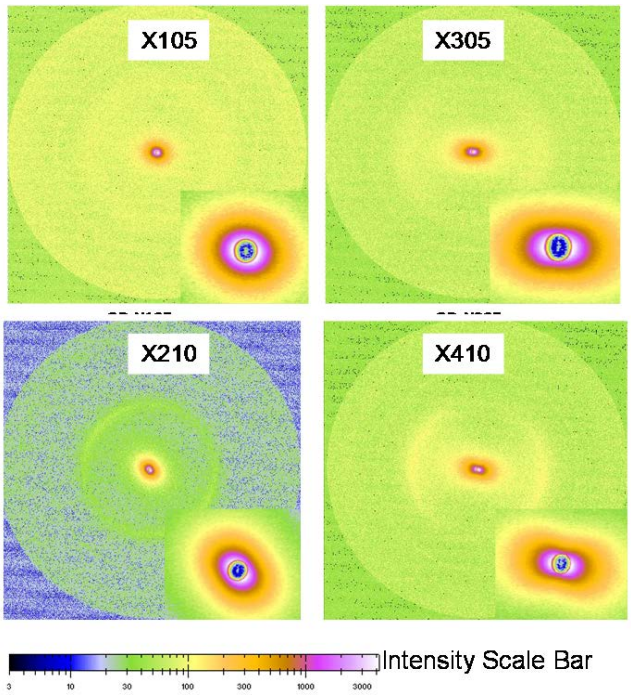

Figure 2 Raw 2-D SAXS patterns for X105/X305 and X210/X410.

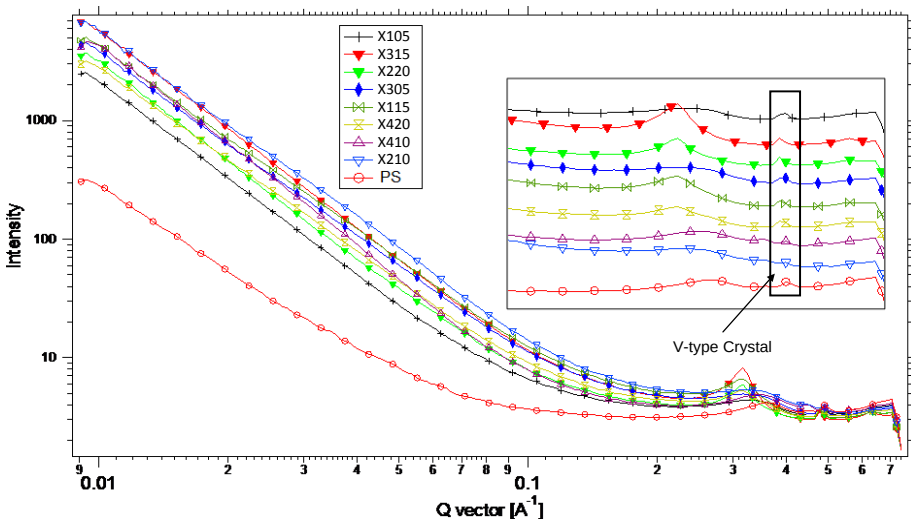

Figure 3 SAXS Profiles for xylitol-plasticized samples.

Table captions

Table 1 Basal spacing, characteristic nanoclay peak position (P_{clay}), glass-transition temperature (T_g) and melting te mperature (T_m) for xylitol-plasticized nanocomposites.

Table 2 The exponent n and the factor k obtained from a non-isothermal crystallization analysis for nanocomposite samples plasticized by xylitol.

Table 3 Radius values (Å) from size distribution calculated by MEM method for xylitol-plasticized low moisture content samples.

Table 1
Basal spacing, characteristic nanoclay peak position (P_{clay}), crystallinity, glass-transition temperature (T_g) and melting temperature (T_m) for xylitol-plasticized nanocomposites.

Sample ID	PS**	X200**	X400**	X105	X115	X210	X220	X305	X315	X410	X420
*Xc** (%)	7.48	8.23	12.5	7.05	11.4	13.4	11.26	9.7	9.34	10.09	9.01
T_g (°C)	49.5	60.17	68.95	55.7	49.6	56.25	39.7	58.5	50.6	50.0	48.6
T_m (°C)	128.5	124.43	120.55	218	204	233	237	133	213	153	246
$P_{clay}(^o)$				5.09	4.73	5.03	4.83	5.2	4.72	4.92	5.02
d-spacing (Å)	-	16.5	18.2	17.3	18.7	17.6	18.3	17.0	18.7	17.9	17.6

*crystallinity calculated from the method described in Lopez-Rubio *et al.* 2008
**reproduced from (Liu, Chaudhary, Yusa & Tadé, 2011b)

Table 2
The exponent n and the factor k obtained from a non-isothermal crystallization analysis for nanocomposite samples plasticized by xylitol.

Sample ID	X105	X115	X210	X220	X305	X315	X410	X420
n	0.62	0.73	0.52	1.50	0.71	1.42	1.11	1.61
k	-1.21	-2.4	-1.69	-1.32	-1.26	-2.38	-2.91	-1.12

Table 3
Radius values (Å) from size distribution calculated by MEM method for xylitol-plasticized low moisture content samples.

Sample ID	$\bar{d}_1$*(Å)	$\bar{d}_2$*(Å)
X105	119.3	357.7
X115	99.7	341.3
X210	98.3	364.1
X220	95.1	345.1
X305	104.2	350.1
X315	101.6	336.2
X410	106.3	348.1
X420	102.3	338.6

* $\bar{d}$: mean scatter diameter (Å)